Supporting information for: Multiflat Bands and Strong Correlations in Twisted Bilayer Boron Nitride: Doping-Induced Correlated Insulator and Superconductor

Lede Xian,[†,‖] Dante M. Kennes,[‡,‖] Nicolas Tancogne-Dejean,[†] Massimo Altarelli,[†] and Angel Rubio[*,†,¶,§]

†*Max Planck Institute for the Structure and Dynamics of Matter, Luruper Chaussee 149, 22761 Hamburg, Germany*

‡*Dahlem Center for Complex Quantum Systems and Fachbereich Physik, Freie Universität Berlin, 14195 Berlin, Germany*

¶*Nano-Bio Spectroscopy Group and ETSF, Universidad del País Vasco UPV/EHU, Avenida de Tolosa 72, E-20018 Donostia, Spain*

§*Center for Computational Quantum Physics (CCQ), The Flatiron Institute, 162 Fifth Avenue, New York, New York 10010, United States*

‖*These authors contributed equally.*

E-mail: angel.rubio@mpsd.mpg.de

Methods

Details about DFT Treatment The ground state DFT calculations are performed with the Vienna Ab initio simulation package (VASP).[1] Plane waves are employed as a basis with an energy cutoff of 400 eV. The pseudo potentials are generated with the projector augmented wave method (PAW)[2] and the exchange-correlation potentials are treated in the local density approximation (LDA).[3] As the system size is relatively large, a 1x1x1 kgrid is employed in the ground state and relaxation calculations. Lattice constants are chosen such that they correspond to a lattice constant of 2.512 Angstrom for a 1x1 unit cell of hBN. During the relaxation, all the atoms are relaxed until the force on each atom is less than 0.01 eV/Angstrom. The VESTA code[4] is used for the visualization of the charge density distributions of the low-energy states of TBBN.

DFT+U calculations The *ab initio* evaluation of the effective U_{eff} and the DFT+U calculations are performed using the Octopus code.[5–8] A real-space spacing of 0.45 Bohr is chosen, and we employ norm-conserving pseudopotentials. The LDA is used for describing the local DFT part, and we utilize the ACBN0 functional to evaluate self consistently the effective U_{eff} of DFT+U. The vacuum size, atomic coordinates and lattice constant are taken to be the same as for the DFT treatment, as described above. Again, only the Gamma point is considered here.

The localized subspace is constructed as a single-shot Wannier states, taking the flat bands from LDA calculations. As the flat bands are energetically separated from the other occupied bands, this implies that the Wannier states reduce to the LDA states at the Gamma point.

The Hubbard-Kanamori parameters U, U' and J are commonly defined from the expression

$$U = \frac{1}{N}\sum_{m}\langle mm|V_{ee}|mm\rangle\,,$$
$$J = \frac{1}{N(N-1)}\sum_{m\neq m'}\langle mm'|V_{ee}|m'm\rangle\,,$$
$$U' = \frac{1}{N(N-1)}\sum_{m\neq m'}\langle mm|V_{ee}|m'm'\rangle\,,$$

where V_{ee} denotes the screened Coulomb interaction. To evaluate these parameters, we extended the definition of the ACBN0 function which yields

$$\bar{U} = \frac{\sum_m \sum_\sigma \bar{P}^{\sigma}_{mm}\bar{P}^{-\sigma}_{mm}(mm|mm)}{\sum_m \sum_\sigma n^{\sigma}_{mm} n^{-\sigma}_{mm}}\,,$$
$$\bar{U}' = \frac{\sum^{*}_{\{m\}} \sum_{\sigma\sigma'} \bar{P}^{\sigma}_{mm'}\bar{P}^{\sigma'}_{m'm''}(mm'|m''m''')}{\sum_{m\neq m'} \sum_\sigma [n^{\sigma}_{mm} n^{\sigma}_{m'm'} + n^{\sigma}_{mm} n^{-\sigma}_{m'm'}]}\,,$$
$$\bar{J} = \frac{\sum^{*}_{\{m\}} \sum_{\sigma} \bar{P}^{\sigma}_{mm'}\bar{P}^{\sigma}_{m'm''}(mm'''|m''m')}{\sum_{m\neq m'} \sum_\sigma n^{\sigma}_{mm} n^{\sigma}_{m'm'}}\,,$$

where $n^{\sigma}_{mm'}$ denotes the density matrix of the localized subspace, $\bar{P}^{\sigma}_{mm'}$ is the the renormalization density matrix (see Ref. 8 for details), and $(mm'|m''m''')$ refers to the Coulomb integrals computed from the bare Coulomb interaction. In the sum over the orbitals $\sum^{*}_{\{m\}}$, the asterisk means that the sum goes over all the orbitals (two here) except for the case in which $m = m' = m'' = m'''$. Importantly, we do not use any symmetry for computing the Coulomb integrals, and evaluate them directly on the real space grid, in order to analyze if the relation $\bar{U} - \bar{U}' = 2\bar{J}$ is fulfilled or not.

We tested both the fully-localized-limit and the around-mean-field double counting terms, and found no sizable change in the value of $U_{\rm eff}$.

Treating Correlations To treat correlations we introduce a tight binding model motivated from the DFT analysis. We want to concentrate on the bands labeled by 3 and 7 in Fig. 2 in the main text. These can be approximated very well by a two band nearest

neighbor tight binding model on a triangular lattice

$$H^0 = -t \sum_{\langle i,j \rangle} \sum_{b=1}^{2} \sum_{\sigma=\uparrow,\downarrow} c^{\dagger}_{i,b,\sigma} c_{j,b,\sigma} - 2t \sum_{i} \sum_{b=1}^{2} \sum_{\sigma=\uparrow,\downarrow} n_{i,b,\sigma}, \tag{1}$$

where $c^{(\dagger)}_{i,b,\sigma}$ annihilates (creates) a particle on site i in the band b and with spin σ and $n_{i,b,\sigma} = c^{\dagger}_{i,b,\sigma} c_{i,b,\sigma}$. The second term (energy-shift) ensures that we measure the chemical potential with respect to van Hove filling for convenience.

We add local Coulomb repulsion and Hund's coupling to this by including

$$\begin{aligned} H^U_i =& U \sum_{b=1}^{2} n_{i,b,\uparrow} n_{i,b,\downarrow} + U' \sum_{\sigma=\uparrow,\downarrow} n_{i,1,\sigma} n_{i,2,-\sigma} + (U' - J) \sum_{\sigma=\uparrow,\downarrow} n_{i,1,\sigma} n_{i,2,\sigma} \\ & - J' \left(c^{\dagger}_{i,1,\downarrow} c^{\dagger}_{i,2,\uparrow} c_{i,2,\downarrow} c_{i,1,\uparrow} + c^{\dagger}_{i,2,\uparrow} c^{\dagger}_{i,2,\downarrow} c_{i,1,\uparrow} c_{i,1,\downarrow} + \text{H.c.} \right) \end{aligned} \tag{2}$$

in the full Hamiltonian $H = H^0 + \sum_i H^U_i$. To reduce the number of parameters we set $J = J'$ and $U' = U - 2J$ (which strictly can be shown to hold for d-orbitals in free space[9]). From our DFT+U estimates we find that this relation is also approximately fulfilled for twisted boron nitride although there seems to be no symmetry argument why this has to be the case. We choose U and J as the two independent parameters to vary in the following, which fixes U'.

The equilibrium phases of the Hamiltonian H can be analyzed in the regime of small to intermediate interaction strength by the well-established functional renormalization group approach (FRG).[10] Similar in spirit to other renormalization groups schemes within this method high-energy degrees of freedom are successively integrated out, resulting in a renormalized, effective low-energy theory of the problem. In our approach we monitor the behavior of the effective two-particle interaction over the flow, which addressed the successive inclusion of high-energy processes into an appropriate effective low energy model. Precursors to ordering tendencies are then indicated by a divergence of the effective two-particle interaction, signaling an instability of the Fermi-surface and a flow to strong coupling.

It is a particular advantage of the functional renormalization group that the method solely takes the Hamiltonian as an input and no a priori identification of dominant interaction channel (e.g. magnetic, superconducting, ...) needs to be made by hand. This allows to treat these different channels on equal footing and thus analyze their competition in an unbiased fashion. As energy scales are successively integrated out over the flow, approaching the chemical potential μ the effective two-particle interaction acquires a strong momentum dependence. It is this momentum dependence combined with the analysis of the diverging channel that allows to draw conclusions about the dominant ordering in the system (varying the parameters of the Hamiltonian). Within the implementation of the FRG we use the implementation of Refs.[10,11] we start the renormalization group flow from the bare two-particle interaction of the Hamiltonian H^U, which shows no momentum dependence (owed to its locality). Therefore, initially (Λ_i denoting the start of the flow) the effective two particle interaction $\Gamma^{\Lambda_i}(k_1, k_2, k_3, \omega_1, \omega_2, \omega_3)$, which in general depends on three independent momenta and frequencies, is momentum and frequency independent. The functional renormalization group approach then provides a recipe of how $\Gamma^{\Lambda}(k_1, k_2, k_3, \omega_1, \omega_2, \omega_3)$ at a different value of the flow parameter Λ can be obtained along the line from Λ_i all the way to Λ_e, which is the end of the flow where the effective low-energy theory of the initial model can be extracted. This is done in terms of rather cumbersome differential equation given in Ref.[10] When an ordering tendency is encountered during this successive flow the effective two-particle interaction $\Gamma^{\Lambda}(k_1, k_2, k_3, \omega_1, \omega_2, \omega_3)$ diverges at a finite Λ_c and the flow needs to be stopped. This Λ_c can roughly be identified with the critical temperature T_c associated with the ordering tendencies.

During the flow (employing momentum and frequency conservation) the effective two-particle interaction depends on three independent momenta as well as three independent frequencies (it is associated with four Fermionic operators, like the bare two-particle interaction). To make the numerical calculation feasible we have to reduce these degrees of freedoms. Since we are interested in the low-energy (equilibrium) physics of the model we

project all frequencies to the chemical potential and all momenta to the Fermi-surface, but keeping their angle dependence, which we discretize in 18 uniform steps from 0 to 2π. For the equilibrium low-energy physics of a system, processes far away from the Fermi-surface are irrelevant, while the angle dependence of the on-shell processes are relevant; justifying this approximation. Therefore in our formulation of the functional renormalization group the low-energy effective two-particle interaction on the Fermi surface is parametrized by the three angles ϕ_1, ϕ_2, ϕ_3 of momenta k_1, k_2, k_3 and thus it can be equivalently written as $\Gamma(\phi_1, \phi_2, \phi_3)$.

When a divergence is encountered in a particular ordering channel of the effective two-particle interaction, with corresponding order parameter $\hat{\Delta}_k$, one can employ a mean-field decomposition

$$\sum_{k,q} = \tilde{\Gamma}^{\Lambda_C}(k,q)[\hat{\Delta}_k, \hat{\Delta}_q] \tag{3}$$

of the dominant contribution to the vertex *after* the flow. The prefactor $\tilde{\Gamma}^{\Lambda_C}(k,q)$ can then be decomposed into the irreducible representation of the underlying lattice model to find the symmetry (e.g. s,p,d,...) of the dominant ordering.

Twisted bilayer system with massive Dirac Hamiltonian

For a twisted bilayer system with each layer being described by a massive Dirac Hamiltonian and a gap of $2m$, we can obtain insights into the evolution of the low-energy band structures by truncating the interlayer hoping matrix and retaining only the leading Fourier components. This truncation implies that we only consider the coupling between the states of the Dirac cone of one layer with the states in the three nearest Dirac cones of the other layer (as

shown in Fig. 1(b)), yielding the following eight-band Hamiltonian:

$$H(\mathbf{k}) = \begin{pmatrix} h_0(\mathbf{k}) & T_1 & T_2 & T_3 \\ T_1^\dagger & h_1(\mathbf{k}_1) & 0 & 0 \\ T_2^\dagger & 0 & h_2(\mathbf{k}_2) & 0 \\ T_3^\dagger & 0 & 0 & h_3(\mathbf{k}_3) \end{pmatrix}, \tag{4}$$

where $\mathbf{k}$ is a small vector within the supercell Brillouin zone and $\mathbf{k}_i = \mathbf{k} + \mathbf{q}_i$ $(i = 1, 2, 3)$, and the h_0 and h_i are the intralayer Hamiltonians of the first and the second layers, respectively, given by:

$$\begin{aligned} h_0(\mathbf{k}) &= \begin{pmatrix} m & vke^{i(\theta_\mathbf{k})} \\ vke^{-i(\theta_\mathbf{k})} & -m \end{pmatrix}, \\ h_i(\mathbf{k}) &= \begin{pmatrix} m & vke^{i(\theta_\mathbf{k}-\theta)} \\ vke^{-i(\theta_\mathbf{k}-\theta)} & -m \end{pmatrix}, \end{aligned} \tag{5}$$

and T_i is the interlayer coupling matrix:

$$\begin{aligned} T_1 = w \begin{pmatrix} 1 & 1 \\ 1 & 1 \end{pmatrix}, T_2 = w \begin{pmatrix} e^{-i\phi} & 1 \\ e^{i\phi} & e^{-i\phi} \end{pmatrix}, \\ T_3 = w \begin{pmatrix} e^{i\phi} & 1 \\ e^{-i\phi} & e^{i\phi} \end{pmatrix}, \end{aligned} \tag{6}$$

where w is the interlayer hopping energy and $\phi = 2\pi/3$. The eigenstates can be written as four two-component spinors $\mathbf{\Psi} = (\psi_0, \psi_1, \psi_2, \psi_3)$, where ψ_0 is located in the subspace of one layer while ψ_i is located in the other.

We can solve the Hamiltonian by treating the momentum as a small perturbation and rewrite $H(\mathbf{k})$ as $H(\mathbf{k}) = H^{(0)} + H^{(1)}(\mathbf{k})$, where $H^{(0)} = H(0)$ and $H^{(1)}(\mathbf{k}) = H(\mathbf{k}) - H(0)$. In zeroth order $\mathbf{k} = 0$, and we find $H^{(0)}\mathbf{\Psi}^{(0)} = \varepsilon^{(0)}\mathbf{\Psi}^{(0)}$. The eigenstates must satisfy the

following equations:

$$h_0(0)\psi_0^{(0)} + T_1\psi_1^{(0)} + T_2\psi_2^{(0)} + T_3\psi_3^{(0)} = \varepsilon^{(0)}\psi_0^{(0)}, \tag{7}$$

$$T_1^\dagger\psi_0^{(0)} + h_1(\mathbf{q}_1)\psi_1^{(0)} = \varepsilon^{(0)}\psi_1^{(0)}, \tag{8}$$

$$T_2^\dagger\psi_0^{(0)} + h_2(\mathbf{q}_2)\psi_2^{(0)} = \varepsilon^{(0)}\psi_2^{(0)}, \tag{9}$$

$$T_3^\dagger\psi_0^{(0)} + h_3(\mathbf{q}_3)\psi_3^{(0)} = \varepsilon^{(0)}\psi_3^{(0)}. \tag{10}$$

From Eqs. (5-7), we find

$$\psi_i^{(0)} = h_i'^{-1}T_i^\dagger\psi_0^{(0)}, \tag{11}$$

where $h_i' = \varepsilon^{(0)} - h_i(\mathbf{q}_i)$. By substituting Eqs. (5),(6) and (11) into Eqn. (4), we can finally show that the eigenenergies for $\mathbf{k} = 0$ must satisfy:

$$(\varepsilon^{(0)} - \frac{6\varepsilon^{(0)}w^2}{(\varepsilon^{(0)})^2 - m^2 - v^2q_0^2})^2 - m^2 = 0, \tag{12}$$

where $q_0 = |\mathbf{q}_i| = |\mathbf{K}_t - \mathbf{K}_b| = 2|\mathbf{K}|sin(\theta/2)$.

When $m << w$, by neglecting all the higher order term of m, the two lowest-energy solutions to Eq. (12) are reduced to:

$$\varepsilon_\pm^{(0)} = \pm m\frac{1}{(1+6\alpha^2)}, \tag{13}$$

where $\alpha^2 = w^2/v^2q_0^2$. Therefore, the band gap of the twisted bilayer system $E_{gap}^{tb} = 2|\varepsilon_\pm^{(0)}|$ is reduced to that of the monolayer $1/(1+6\alpha^2)$. With large twist angle when $vq_0 >> w$, the band gap E_{gap}^{tb} is approaching the monolayer value; while in the limit $\theta \to 0$, $\alpha^2 \to \infty$, thus $E_{gap}^{tb} \to 0$, which indicates that the band gap could be closed at small twist angle.

When $m >> w$ and $m >> vq_0$ (twist angle is small), the lowest eigenenergies can be

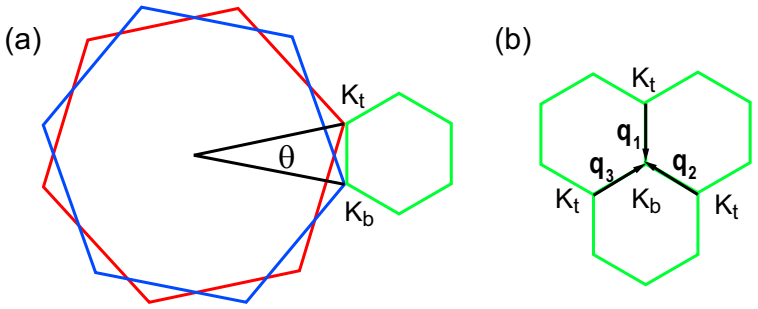

Figure 1: (a) Brillouin zones of the top layer (in red), the bottom layer (in blue) and the twisted system in a supercell (in green). (b) Reciprocal geometry of the K point of the bootom layer and the three nearest K points of the top layers in the supercell Brillouin zone. The three correponding vectors that connect the K points are: $\mathbf{q}_1 = (0, -1)q_0$, $\mathbf{q}_2 = (\sqrt{3}/2, -1/2)q_0$, and $\mathbf{q}_3 = (\sqrt{3}/2, 1/2)q_0$.

approximately reduced as:

$$\varepsilon_{\pm}^{(0)} = \pm(m + v^2 q_0^2/4m - \sqrt{3}w). \tag{14}$$

In the small angle limit when $\theta \to 0$, the band gap is approaching the limit of $2m - 2\sqrt{3}w$, which means that the band gap will never be closed in this case.

For $\mathbf{k} \neq 0$, the correction to the eigenenergies up to the first order in k can be obtained by:

$$\begin{aligned} &\langle \mathbf{\Psi}^{(0)} | H^{(1)}(\mathbf{k}) | \mathbf{\Psi}^{(0)} \rangle \\ &= \frac{v}{N^2} \psi_0^{(0)\dagger} [\sigma \cdot \mathbf{k} + \sum_i T_i h_i'^{-1\dagger} \sigma \cdot \mathbf{k} h_i'^{-1} T_i^\dagger] \psi_0^{(0)} \\ &= (v_1^* - v_2^* i\sigma_z) \psi_0^{(0)\dagger} \sigma \cdot \mathbf{k} \psi_0^{(0)}, \end{aligned} \tag{15}$$

where N^2 is the normalization factor

$$\begin{aligned} N^2 &= \langle \mathbf{\Psi}^{(0)} | \mathbf{\Psi}^{(0)} \rangle \\ &= 1 + \frac{6(\varepsilon^2 + m^2 + v^2 q_0^2) w^2}{(\varepsilon^2 - m^2 - v^2 q_0^2)^2}, \end{aligned} \tag{16}$$

and

$$v_1^* = \frac{v}{N^2}[1 + \frac{3w^2}{(\varepsilon^{(0)})^2 - m^2 - v^2q_0^2}],$$
$$v_2^* = \frac{v}{N^2}\frac{6w^2\varepsilon^{(0)}vq_0}{((\varepsilon^{(0)})^2 - m^2 - v^2q_0^2)^2}. \tag{17}$$

The first term v_1^* in the Eq. (15) denotes the Dirac velocity renormalization and the second term $-v_2^* i\sigma_z$ is a small correction related to a 90° rotation of the momentum $\mathbf{k}$. When $m = 0$, $\varepsilon_\pm^{(0)} = 0$ according to Eq. (13), then we have $v_2^* = 0$ and $v_1^* = \frac{1-3\alpha^2}{1+6\alpha^2}v$, which is the well-known Fermi velocity renormalization behavior in twisted bilayer graphene. The condition of $1 - 3\alpha^2 = 0$ signals the changing of sign of Dirac velocity v_1^* and gives the value of the first magic angle.

For the lowest energy eigenstates, we can further reduced v_1^* to the following form using the relation in Eq. (12):

$$v_1^* = \frac{v}{2N^2}(3 \mp \frac{m}{\varepsilon_\pm^{(0)}}). \tag{18}$$

When $m << w$, we can substitute Eq. (13) into Eq. (18) yielding

$$v_1^* = v(1 - 3\alpha^2)/N^2. \tag{19}$$

Therefore, v_1^* changes sign also at $1 - 3\alpha^2 = 0$ and the twisted bilayer massive Dirac system shares the same first magic angle as twisted bilayer graphene. When $m >> w$, from Eqs. (14) and (18), we obtain

$$v_1^* = \frac{v}{2N^2}(3 - 1/(1 + \frac{v^2q_0^2}{4m^2} - \frac{\sqrt{3}w}{m})). \tag{20}$$

From the above expression, we see that v_1^* is always larger than 0 as long as $w/m < 2/(3\sqrt{3}) \approx 0.38$. There is no magic angle when the size of the monolayer gap ($2m$) is much larger than twice the interlayer coupling energy ($2w$).

In TBBN, the size of the band gap of monolayer is calculated to be 4.7 eV in LDA, which is much larger than twice of interlayer coupling energy (less than 0.6 eV), so it is expected that the Dirac velocities at the band edges will not change sign as twist angle decreases and

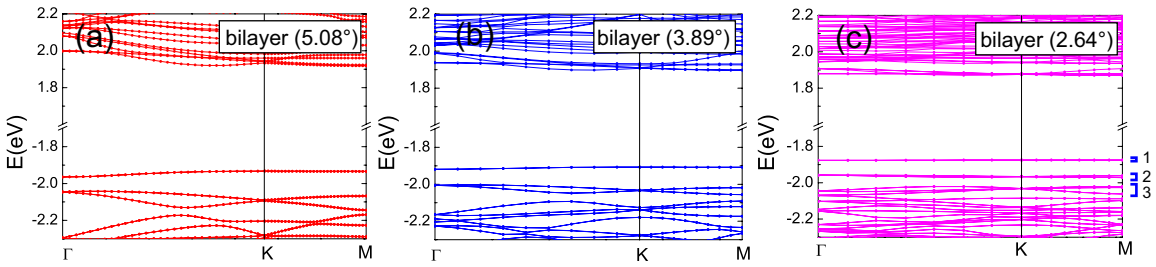

Figure 2: Evolution of the band structure of unrelax TBBN with different twist angles: (a) 5.08°, (b) 3.89°, and (c) 2.64°.

there are no magic angles in TBBN.

Doping density required to achieve half-filling in TBBN

The general relation between the Moire period D and the lattice constant a_0 of the original lattice is:

$$D = a_0/(2sin(\frac{\alpha}{2})) \approx a_0/\alpha, \tag{21}$$

where $a_0 = 2.512$ in the DFT calculation for hBN, α is the twist angle. The top valence flat bands can host up to 4 electrons per Moire supercell. Therefore, the doping density required to achieve half-filling for the first flat band is (see also Fig. 4):

$$n = \frac{2}{A} = \frac{2}{\frac{\sqrt{3}D^2}{2}} = \frac{4\alpha^2}{\sqrt{3}{a_0}^2}, \tag{22}$$

where A is the area of the supercell. When the twist angle α decreases, the doping density required to achieve half-filling in TBBN will be significantly decreased.

References

(1) Kresse, G.; Hafner, J. Ab initio molecular dynamics for liquid metals. *Phys. Rev. B* **1993**, *47*, 558.

(2) Blöchl, P. E. Projector augmented-wave method. *Phys. Rev. B* **1994**, *50*, 17953.

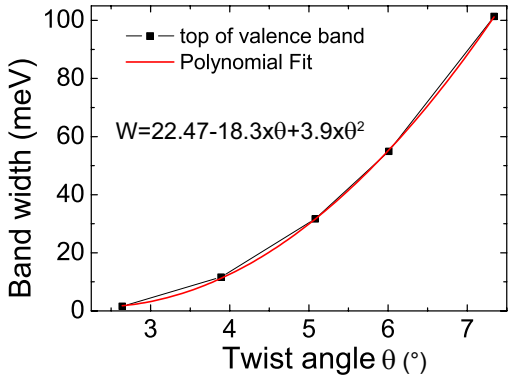

Figure 3: Polynomial fitting of the band width of the top of valence bands in unrelax TBBN with twist angle larger than 2.64 degrees.

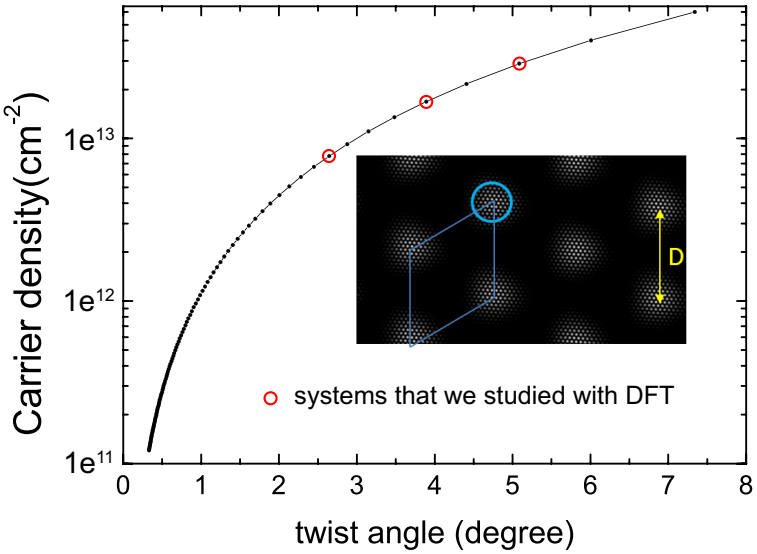

Figure 4: Doping density required to achieve half-filling in TBBN with different twist angles. Inset shows the Moire supercell with period D.

(3) Perdew, J. P.; Zunger, A. Self-interaction correction to density-functional approximations for many-electron systems. *Phys. Rev. B* **1981**, *23*, 5048.

(4) Momma, K.; Izumi, F. VESTA 3 for three-dimensional visualization of crystal, volumetric and morphology data. *J. Appl. Crystallogr.* **2011**, *44*, 1272–1276.

(5) Marques, M. A.; Castro, A.; Bertsch, G. F.; Rubio, A. Octopus: a first-principles tool for excited electron-ion dynamics. *Comput. Phys. Commun.* **2003**, *151*, 60 – 78.

(6) Castro, A.; Appel, H.; Oliveira, M.; Rozzi, C. A.; Andrade, X.; Lorenzen, F.; Mar-

ques, M. A. L.; Gross, E. K. U.; Rubio, A. Octopus: a tool for the application of time-dependent density functional theory. *Phys. Status Solidi (b)* **2006**, *243*, 2465–2488.

(7) Andrade, X. et al. Real-space grids and the Octopus code as tools for the development of new simulation approaches for electronic systems. *Phys. Chem. Chem. Phys.* **2015**, *17*, 31371–31396.

(8) Tancogne-Dejean, N.; Oliveira, M. J. T.; Rubio, A. Self-consistent DFT$+U$ method for real-space time-dependent density functional theory calculations. *Phys. Rev. B* **2017**, *96*, 245133.

(9) Werner, P.; Millis, A. J. High-Spin to Low-Spin and Orbital Polarization Transitions in Multiorbital Mott Systems. *Phys. Rev. Lett.* **2007**, *99*, 126405.

(10) Metzner, W.; Salmhofer, M.; Honerkamp, C.; Meden, V.; Schönhammer, K. Functional renormalization group approach to correlated fermion systems. *Rev. Mod. Phys.* **2012**, *84*, 299–352.

(11) Kennes, D. M.; Lischner, J.; Karrasch, C. Strong correlations and $d + id$ superconductivity in twisted bilayer graphene. *Phys. Rev. B* **2018**, *98*, 241407.